Electrochimica Acta 292 (2018) 425–434

Contents lists available at ScienceDirect

Electrochimica Acta

journal homepage: www.elsevier.com/locate/electacta

Influences of semiconductor oxide fillers on the corrosion behavior of metals under coatings

Sijia Li, Wen Sun, Zhengqing Yang, Xinyu Zhang, Lida Wang, Guichang Liu*

Department of Materials Science and Chemical Engineering, Dalian University of Technology, No. 2 Linggong Road, Dalian 116024, China

ARTICLE INFO

Article history:
Received 28 May 2018
Received in revised form
17 August 2018
Accepted 17 August 2018
Available online 21 September 2018

Keywords:
Organic coatings
Semiconductor oxide
Localized EIS
Work function

ABSTRACT

Semiconductor oxides are widely used as coating fillers, while few studies have focused on the interactions between semiconductor fillers and metal substrates. In this paper, common semiconductor fillers including TiO_2, Fe_2O_3 and Cu_2O were prepared and incorporated into polyvinyl butyral coatings. Localized EIS, EIS, SEM and electrochemical noise analysis were applied to study the corrosion behavior of semiconductor/metal contacts at coating defects. Results revealed that TiO_2 and Fe_2O_3 accelerated the corrosion of metals, while Cu_2O showed no promising effect. Meanwhile, a micro-galvanic corrosion mechanism based on work function difference and oxygen reduction reaction activity was proposed to explain the corrosion-promotion phenomenon.

© 2018 Elsevier Ltd. All rights reserved.

1. Introduction

Galvanic corrosion, which is attributed to an electrical contact with a more noble metal or nonmetallic conductor in corrosive electrolyte, is a major concern that may bring about severe corrosion damage and metal structure failure [1]. Recently, it has been reported that one of the main sources of galvanic corrosion is the electrical contact between metal and semiconductor [2]. Moreover, researches have revealed that some corrosion products such as iron sulfides [3], iron carbide [4] and iron carbonate [5] showed significant promotion effect on the corrosion behavior of metal substrates. In previous studies, such a corrosion occurring beneath the thick and porous corrosion production layer was believed as under-deposit corrosion. However, recent researches have demonstrated that the micro-galvanic cell between semiconductive corrosion products and metal is an important cause of corrosion acceleration as well [6]. For example, Bai et al. [7] revealed that the formation of iron sulfide (FeS), a sort of corrosion product, contributed markedly to the sharp increase in corrosion rate of carbon steel because semiconductive FeS is an electrochemically active material with a more noble potential than steel. Similarly, Song et al. [8,9] reported that some corrosion products (such as Fe_2O_3 and FeOOH) were able to accelerate the atmospheric corrosion of metals in the presence of UV illumination. They believed that the photo-induced holes in semiconductive corrosion product could directly capture the electrons from metal substrates and thus improved the atmospheric corrosion rates of the metals.

Not only some semiconductor materials can accelerate metal corrosion, it has been reported that metals have a great influence on corrosion behavior of semiconductor as well [10–12]. Meanwhile, a series of semiconductor-metal nanostructures have been widely applied to various areas such as photocatalytic operation [13] and photodetectors [14] due to different Fermi level (E_F) between semiconductors and metals rather than their potential difference [15,16]. Zhang et al. [17] investigated that contact electrification of metal assisted chemical etching in three dimensional micro-nanostructures fabrication between Pt and n-GaAs can induce interfacial redox reactions, and they explained this phenomenon through work function difference between Pt and n-GaAs. When the Pt electrode comes into contact with n-GaAs, electrons of n-GaAs will be deprived by Pt and form a contact electric field at the Pt/n-GaAs junction. Therefore, it can be concluded that the interaction between semiconductor and metal is a common phenomenon; however, it has not attracted a wide attention in corrosion field because there is few general explanation about the transfer of electrons at semiconductor-metal interfaces.

Nowadays, semiconductor oxide materials have been widely used as functional fillers to confer coatings with superior physical and chemical properties [18–21]. Moreover, some studies revealed

* Corresponding author.
E-mail address: gchliu@dlut.edu.cn (G. Liu).

https://doi.org/10.1016/j.electacta.2018.08.116
0013-4686/© 2018 Elsevier Ltd. All rights reserved.

that some coatings with high pigment volume concentrations had a higher corrosion resistance and a better mechanical performance [22,23]. Thus, it should be taken into consideration that semiconductor fillers embedded in the coatings are able to interact with metal substrates. However, up till now, there have been few reports on the interactions between semiconductor fillers and metal substrates beneath coatings. In our previous work, we already demonstrated that semiconductive α-Mn_2O_3 filler was able to catalyze the oxidation of copper [24]. It was supposed to be associated with the oxygen reduction reaction (ORR) catalytic activity of α-Mn_2O_3 and the Ohmic contact fabricated at the semiconductor filler/metal interface. In addition, we also observed that the N-doped graphene filler with high ORR activity could accelerate corrosion of substrates [25]. It can be concluded that semiconductor fillers may possess a significant effect on the corrosion behavior of metal substrates at coating defects, which has a further perspective in investigation of corrosion reaction between metal and oxide materials such as some corrosion products and oxide films formed on metals.

In this paper, in order to demonstrate the universality of the corrosion-promotion phenomenon, three typical fillers including TiO_2, Fe_2O_3 and Cu_2O were chosen to investigate whether they have impact on the corrosion behavior of metal substrates or not. Localized EIS (LEIS), EIS, SEM and electrochemical noise analysis were used to study the corrosion behavior of semiconductor/metal contacts at coating defects. Furthermore, an appropriate mechanism based on the work function difference between semiconductor oxides and metals and the ORR activity of semiconductor fillers was proposed to explain the corrosion-promotion activity of semiconductor fillers. This paper also has general guiding significance for choosing semiconductor oxides as coating fillers.

2. Experimental

2.1. Fabrication of semiconductor oxides

2.1.1. Synthesis of TiO_2

$Ti(SO_4)_2$ and $CO(NH_2)_2$ were dissolved in 50 mL deionized water with molar ratio of 0.1:1. Then the solution was poured into a teflon-lined autoclave and hydrothermally heated at 130 °C for 1.5 h. Next, the slurry that contains TiO_2 particles was separated by a centrifuge, and sequently washed with deionized water until SO_4^{2-} cannot be detected. The obtained product was finally dried at vacuum at 70 °C.

2.1.2. Synthesis of Fe_2O_3

Ferric nitrate ($Fe(NO_3)_3$) and urea ($CO(NH_2)_2$) were homogeneously mixed with a molar ratio of 1:1.5 in 50 mL deionized water, and hydrothermally maintained at 200 °C for 4 h. The urea was found to decompose into ammonia and carbon dioxide at 70 °C, acting as precipitation agent. The filtered powders were then washed with deionized water and dried at 110 °C in air.

2.1.3. Synthesis of Cu_2O

0.057 g $CuCl_2 \cdot 2H_2O$ were dissolved in 50 mL of 3 M NaOH solution in an ultrasonic bath, forming a transparent blue $Cu(OH)_4^{2-}$ solution. Then 1.093 g cetyltrimethyl ammonium bromide was added to the solution and magnetically stirred for 30 min to obtain a homogeneous solution. 0.079 g D-glucose was added into the solution and then magnetically stirred for another 10 min. After that, the mixed solution was transferred into a 50 °C water bath for 10 min. The precipitations were separated by add centrifugation and washed with distilled water and absolute ethanol several times and dried at vacuum at 40 °C for 5 h.

2.2. Preparation of coatings

0.5g TiO_2, Fe_2O_3 and Cu_2O powders were dispersed in 7.5 g methanol separately by ultrasonic dispersion for 1 h, then stirred for 24 h to produce uniform dispersion. Next, 1 g polyvinyl butyral (PVB) powders (Sinopharm Chemical Reagent Co., Ltd.) were added to the dispersion (Calculation reveals that the pigment volume concentration (PVC) of TiO_2/PVB coating, Fe_2O_3/PVB coating and Cu_2O/PVB coating were 11.23%, 9.26% and 8.19% at the pigment/binder ratio of 1:2, respectively). Finally, the semiconductor/PVB coatings were obtained by stirring the sticky mixture for 8 h and let it stand for 24 h. Besides, a blank PVB coating was also prepared. As a matter of convenience, all the coatings were defined as BPc (blank PVB coating), TPc (TiO_2/PVB coating), FPc (Fe_2O_3/PVB coating) and CPc (Cu_2O/PVB coating), respectively.

2.3. Preparation of samples

The metal samples with an exposed area of 10 mm × 10 mm were embedded in an epoxy resin. The samples were mechanically grounded with silicon carbide (SiC) emery papers down to 1200 grit and washed with water. After that, the coatings were fabricated on the surface of the substrates through a dip-coating method. The metal substrates were immersed in coatings for 30 s, and then withdrawn from the dispersion at a speed of 0.5–1 mm/s to make sure the different coatings have the same thickness. The thickness of coatings were in the range of 30 ± 1.5 μm. In the center of the samples, an artificial scratch (10 mm long and 0.2 mm width) was made to investigate the effect on the corrosion behavior of metal substrates at the coating defects. Finally, the scratched samples were immersed in 3.5 wt % NaCl solution for 1 h before electrochemical tests.

2.4. Characterization

The crystal structures of semiconductor oxides were characterized by X-ray diffraction (XRD, Empyrean, Holland). The morphology and dimensions of semiconductor oxides were determined by scanning electron microscopy (SEM, ZEISS Ultra 55, Germany). SEM was also employed to characterize the surface morphology of corrosion products formed on the scratches of substrates. The work functions of semiconductor oxides and copper were measured by Scanning Kelvin Probe (Model 470 Scanning Electrochemical Workstation).

2.5. Electrochemical tests

Localized electrochemical impedance spectroscopy (LEIS) measurements were performed on working electrode through a PAR Model 470 Scanning Electrochemical Workstation which was comprised of a SCV 470 control unit, a SP-300 Potentiostat, a high impedance input amplifier using a differential electrometer and a probe scanning assembly drives in 'X', 'Y', 'Z' directions. The microprobe was stepped over a designated area (2 mm × 2 mm) of the electrode surface. The schematic diagram of LEIS apparatus and working electrode are shown in Fig. 2a and b, respectively. The scanning took the form of a raster in x–y plane. The dimension of the scratches on the x axis is from 900 to 1100 μm. The distance between the probe-tip and the sample surface was approximately 60 μm, which was adjusted and monitored through a video camera system. The AC disturbance signal was 10 mV, and the excitation frequency for impedance measurements was fixed at 1 Hz.

Electrochemical impedance spectroscopy (EIS) test was conducted on a CHI 750e electrochemical workstation (Shanghai Chenhua Device Company, China) with a three-electrode system,

which consists of a platinum wire used as an auxiliary electrode, a saturated calomel electrode (SCE) as reference electrode and the tested sample as working electrode. EIS was performed on the substrates covered by scratched semiconductor/PVB coatings as well as BPc during 1 week of immersion in 3.5 wt % NaCl solution. The frequency ranged from 10 mHz to 100 kHz, with a signal amplitude of 10 mV.

The conventional electrochemical noise (EN) test was measured on a CS310 electrochemical workstation (Wuhan CorrTest Device Company, China) by three electrodes. Two working electrodes were made of the same material, and a SCE reference electrode was used so that the two working electrodes were at the same potential. Before the EN test, the scratched substrates were immersed in 3.5 wt % NaCl solution for 12 h. The potential noise was tested one point per second during a time period of 1024 s for data storage and analysis. EN has been performed for data obtained in the time and the frequency domains.

The linear sweep voltammetry (LSV) measurement has been applied to investigate the ORR performance of semiconductor oxides. With the help of CHI 750e electrochemical workstation, the rotating-disk electrode (RDE) was carried out in O_2-saturated 3.5 wt % NaCl solution. For the RDE measurement, 5 mm glassy carbon disk was used as a working electrode. The diffusion current density improved with the increased rotation rate from 200 to 1600 rpm due to the enhanced mass transfer in the electrolyte.

Copper substrates were used in LEIS and EIS measurements, and

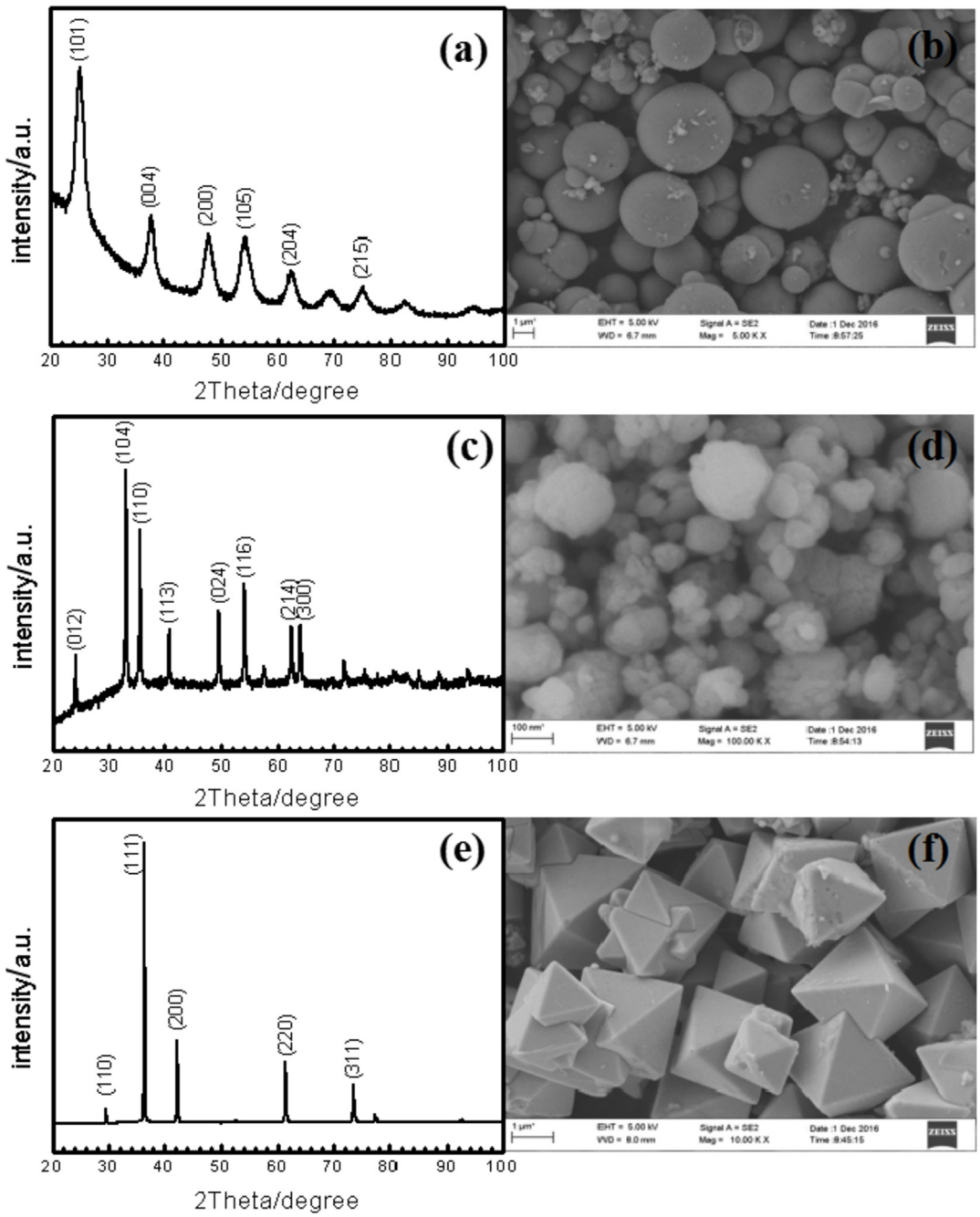

Fig. 1. (a), (c) and (e) XRD patterns of the synthesized TiO_2, Fe_2O_3 and Cu_2O, (b), (d) and (f) SEM images of the synthesized TiO_2 microspheres, Fe_2O_3 nanoparticles and octahedral Cu_2O.

the EN measurement was performed on Al alloy specimens. All electrochemical tests were repeated at least three times to guarantee repeatability.

3. Results and discussion

3.1. Morphology and structure of semiconductor materials

Fig. 1 shows the XRD patterns of semiconductor materials prepared by different chemical methods. Fig. 1a indicates that all the marked peaks can be well indexed to the standard pattern of anatase TiO_2 (JCPCDS Card NO.21-1272) without any impurities. Fig. 1c shows that all diffraction peaks of as-prepared Fe_2O_3 match the standard pattern of the six-party hematite structure (JCPCDS Card NO.33-0664). The strong and sharp diffraction peaks in Fig. 1e also demonstrate that Cu_2O forms a pure octahedral structure corresponding to the standard pattern (JCPCDS Card NO.05-0667). The morphologies and sizes of the semiconductor products are studied by SEM to get a better observation as shown in Fig. 1. Fig. 1b shows that the obtained TiO_2 powder is composed of microspheres with diameters of 1–2 μm. The Fe_2O_3 nanoparticles are less than 100 nm in size as presented in Fig. 1d. Fig. 1f reveals that the as-prepared Cu_2O particles are octahedrons with edge lengths of 1–2 μm.

3.2. Corrosion behavior of scratched specimens

The interaction between semiconductor oxide fillers and metal substrates can be evaluated by LEIS measurement. In this work, LEIS mappings of the areas around the artificial defect of the four different coatings were performed by measuring the local impedance at a frequency of 1 Hz during 1 h of immersion. The principles of LEIS are similar to those employed in conventional EIS, i.e., a small sinusoidal voltage perturbation is applied to a working electrode sample, and the resulting current is measured to calculate impedance. Contrary to conventional EIS, LEIS enables the investigation of the local zones of a working electrode [26]. The sketch map of an LEIS apparatus is shown in Fig. 2a. The five-electrode arrangement consists of a typical three-electrode arrangement [working electrode (WE), counter electrode (CE), and reference

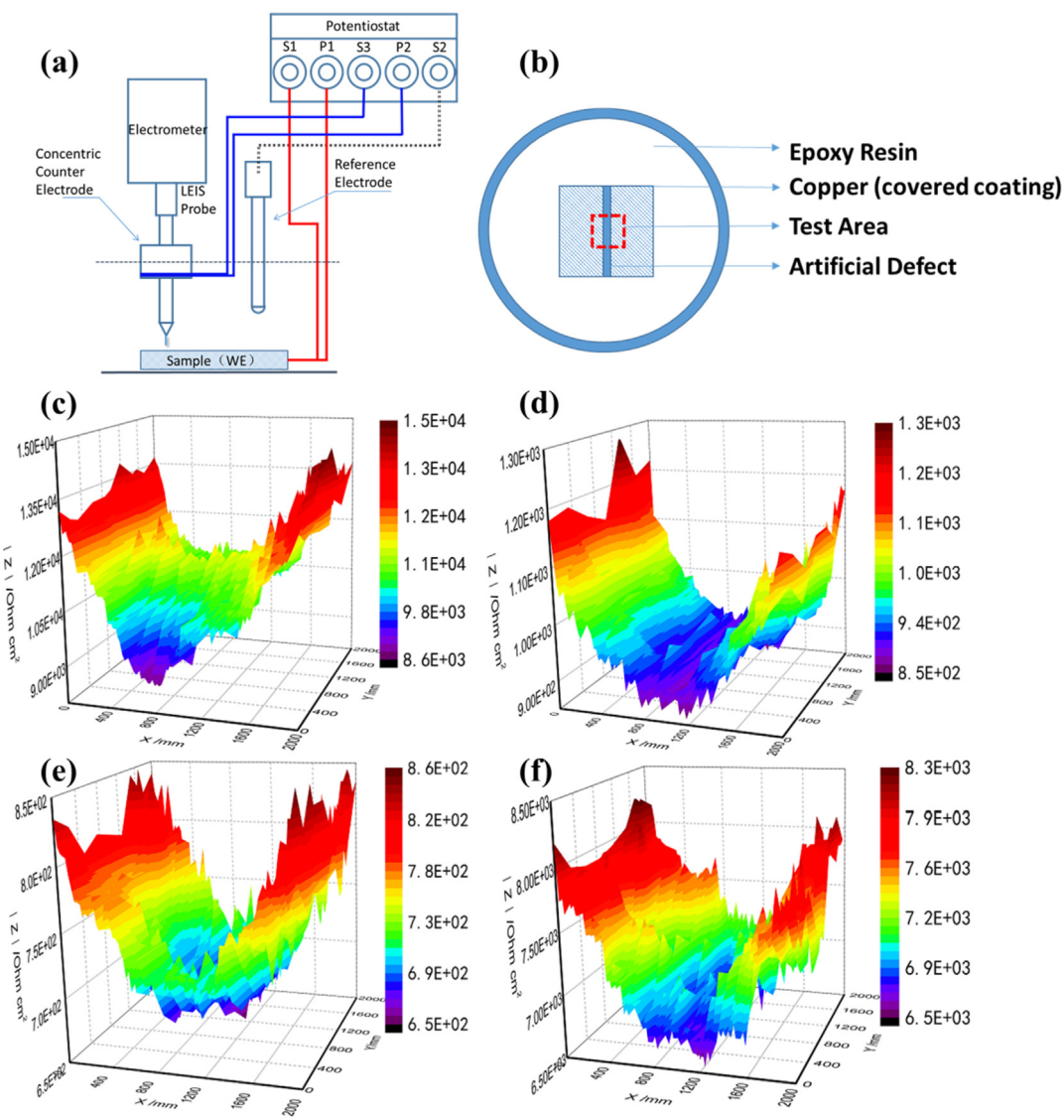

Fig. 2. (a) Schematic diagram of LEIS apparatus, (b) schematic diagram of working electrode. LEIS maps around the defective area of (c) BPc, (d) TPc, (e) FPc and (f) CPc after 1 h immersion.

electrode (RE)], while two micro "reference" electrodes are used to detect the local potential gradient in the solution. The counter electrode and two micro "reference" electrodes form the probe of the LEIS apparatus. The two micro "reference" electrodes consists of Teflon-coated platinum wires, which are positioned on and in a conical plastic holder. One of the micro "reference" electrodes protrudes from the tip of the cone, and the other is a ring placed around the cone 3 mm from the tip. For LEIS mapping the probe was stepped across a well-defined area of the sample that depicted in Fig. 2b. The color intensity characterizes the distribution of the impedance values at the sample surface. It is clear that the defect area in the coated electrode generates the lowest impedance value in the map. As shown in Fig. 2c and f, impedance values at the defects of BPc and CPc are about $8.6 \times 10^3\,\Omega\,cm^2$ and $6.5 \times 10^3\,\Omega\,cm^2$, respectively, while the lowest impedance values measured on the defects of TPc and FPc are approximately $8.5 \times 10^2\,\Omega\,cm^2$ and $6.5 \times 10^2\,\Omega\,cm^2$ (Fig. 2d and e). The figures indicate that impedance values of BPc and CPc are ten times larger than that of TPc and FPc. The LEIS mappings confirm that electrochemical reactivity on the defects of BPc and CPc are lower than that of TPc and FPc. It suggests that the presence of TiO_2 and Fe_2O_3 improves corrosion development, increasing the local anodic activity at the exposed areas. The LEIS results reveal that, compared with BPc and CPc, the substrates beneath TPc and FPc suffered more severe corrosion. Therefore, it can be concluded that TiO_2 and Fe_2O_3 possess corrosion-promotion activity, whereas Cu_2O does not.

EIS is one of the most effective techniques to characterize the corrosion resistance of coated metals. The EIS plots of copper specimen are also presented in this section to demonstrate the corrosion-promotion activity of semiconductor oxides. Fig. 3a–d shows the original and fitted Bode plots and the fitted results of charge transfer resistance (R_{ct}) of the scratched specimens after 7 days immersion in 3.5 wt% NaCl aqueous solution. The Bode modulus plots show that different coatings exhibit different magnitude of the impedance which correspond to corrosion resistance. Usually, the impedance moduli at low frequencies generally reflect the protective properties of coatings, so $|Z|_{0.01\,Hz}$ values were applied to generally distinguish different responses of copper corrosion of four coatings. The Bode-modulus plots of BPc and CPc show a high $|Z|_{0.01\,Hz}$ value (approximately $1.3 \times 10^4\,\Omega\,cm^2$ and $9.3 \times 10^3\,\Omega\,cm^2$) after 7 days' immersion. While for TPc and FPc, the $|Z|_{0.01\,Hz}$ values are about $1.7 \times 10^3\,\Omega\,cm^2$ and $1.3 \times 10^3\,\Omega\,cm^2$, respectively, indicating that BPc and CPc exhibit better barrier properties against corrosive species compared with TPc and FPc. Therefore, it can be concluded that TiO_2 and Fe_2O_3 accelerate the electron transfer process in the interface between copper substrates and coatings.

In order to quantitatively assess the influence of different semiconductor oxides on the corrosion behavior of copper substrates, the EIS results were further analyzed on the ZSimpWin software using the equivalent circuits showed in Fig. 3c. For scratched coatings, the electrochemical corrosion process at the metal surface consists of a double-layer capacitance (Q_{dl}) and a charge transfer resistance (R_{ct}). On the consideration that the electrochemical behaviors of systems do not correspond to pure capacitors, all the capacitors shown in the equivalent electrical circuits are mathematically modeled using a constant phase element (CPE) [27]. The fitted results are shown in Fig. 3d. For the substrates coated by BPc and CPc, the values of resistance after 7 days' immersion are about $1.6 \times 10^4\,\Omega\,cm^2$ and $1.4 \times 10^4\,\Omega\,cm^2$, respectively. The fitted results of the EIS data show that the R_{ct} values of the copper coated by TPc ($2.0 \times 10^3\,\Omega\,cm^2$) and FPc ($1.7 \times 10^3\,\Omega\,cm^2$) are roughly the same, which are apparently less than those of BPc and CPc coated substrates. The EIS results are in

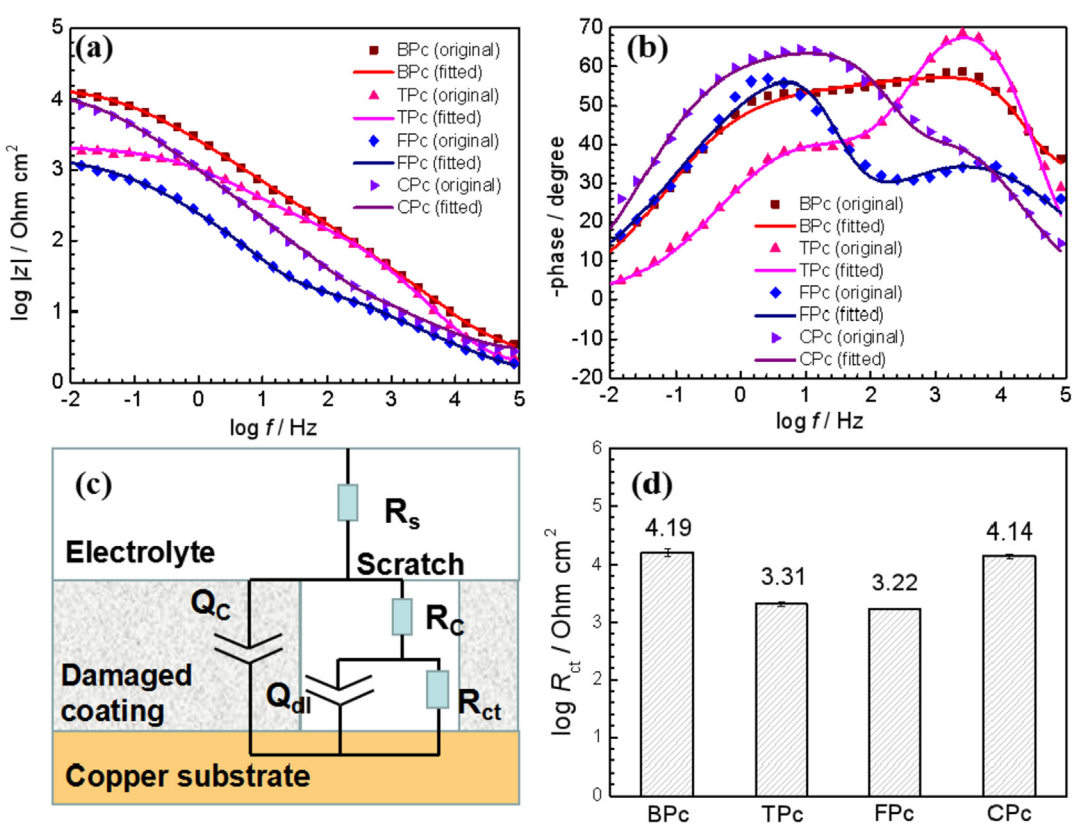

Fig. 3. (a) (b) Original and fitted Bode plots of the coatings immersed in 3.5 wt% NaCl aqueous solution for 7 days, (c) Equivalent circuit and (d) the fitted R_{ct} results of different coatings.

good agreement with the LEIS results, which reveal the more intense corrosion activity of TPc and FPc.

SEM images of the scratches on copper substrates after 7 days of immersion in 3.5 wt% NaCl are shown in Fig. 4. As shown in Fig. 4a and d, no corrosion product deposited in the scratched areas of BPc and CPc can be observed. However, the scratches of coppers coated by TPc and FPc are almost completely filled with corrosion products (Fig. 4b and c), demonstrating that a severe corrosion occurred on the copper substrates. Therefore, the SEM images further confirm that, in comparison with BPc, TPc and FPc have a stronger corrosion-promotion activity, while CPc does not possess corrosion-promotion activity.

EN technology was used to continuously monitor the process of metal corrosion in NaCl solution. Our experiments reveal that EN signal of aluminum is much more obvious than that of copper. The EN data of scratched aluminum sheets are presented in this paper because EN signal obviously reflects the characteristic changes of local corrosion [28,29]. Once the corrosion behavior changes, it will be rapidly detected by potential noise wave obviously. As shown in Fig. 5, the potential noise after eliminating DC signal of TPc and FPc shows a violent fluctuation throughout the whole experiment. However, the evolution of the potential noise of CPc is similar to that of BPc, and the potential wave frequency is much smaller than that obtained on TPc and FPc. It has also been demonstrated that the rising and falling of the potential noise represent destruction and repassivation process of metallic passive film, respectively; an increase of quantity and frequency of the potential transients confirm an active reaction and severe corrosion on the electrode surface [30,31]. It is revealed that the corrosion reactions at TPc and FPc surfaces are more active and intense than others.

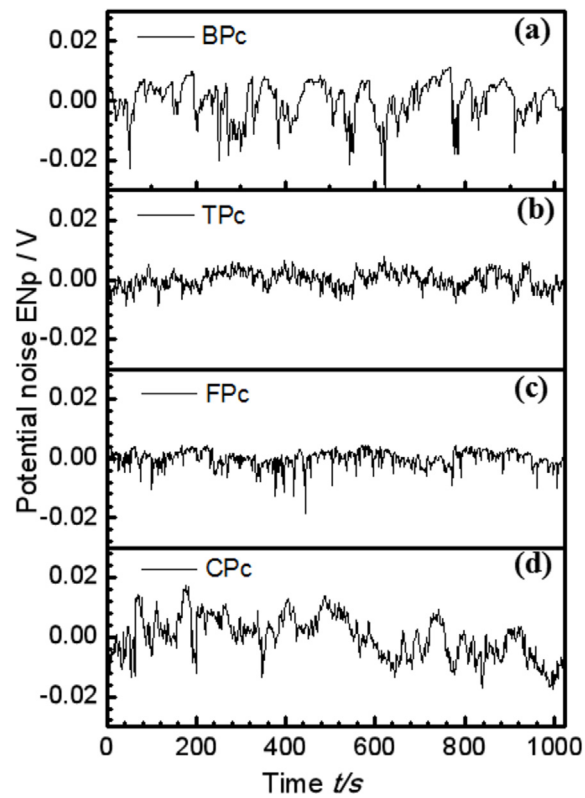

Fig. 5. Potential noise of (a) BPc, (b) TPc, (c) FPc and (d) CPc in 3.5 wt% NaCl aqueous solution.

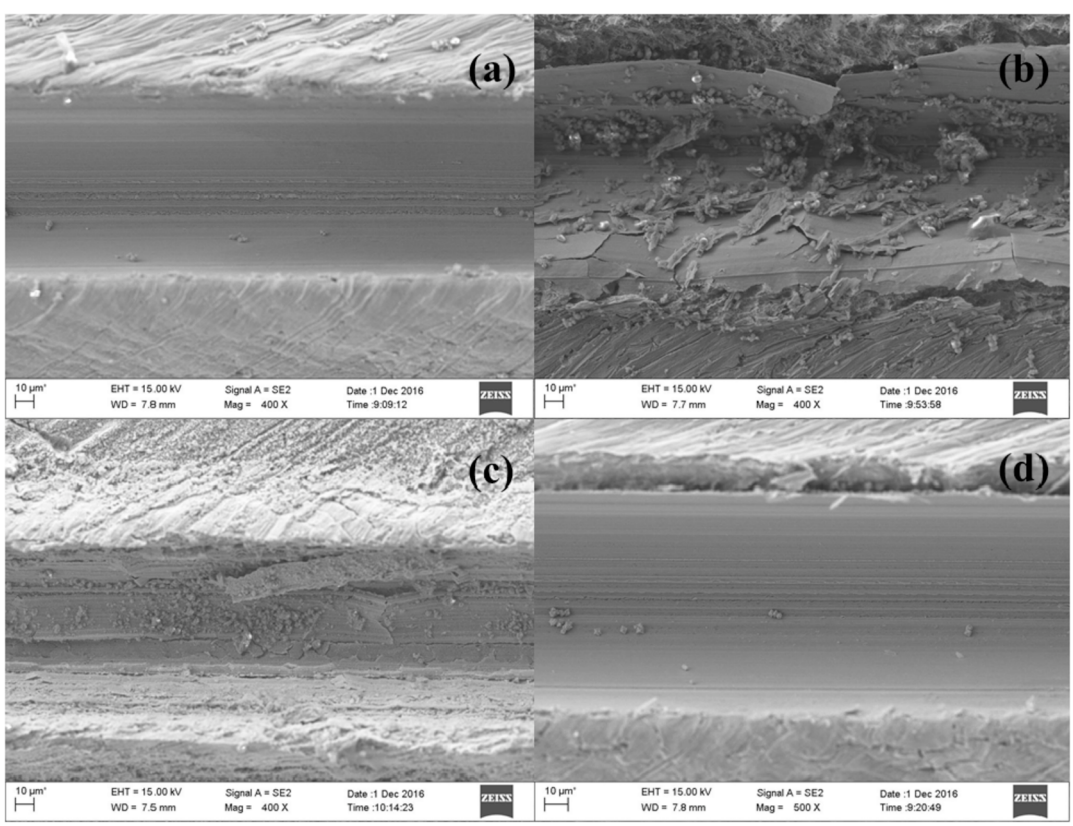

Fig. 4. SEM images of the scratched copper substrates coated by (a) BPc, (b) TPc, (c) FPc and (d) CPc.

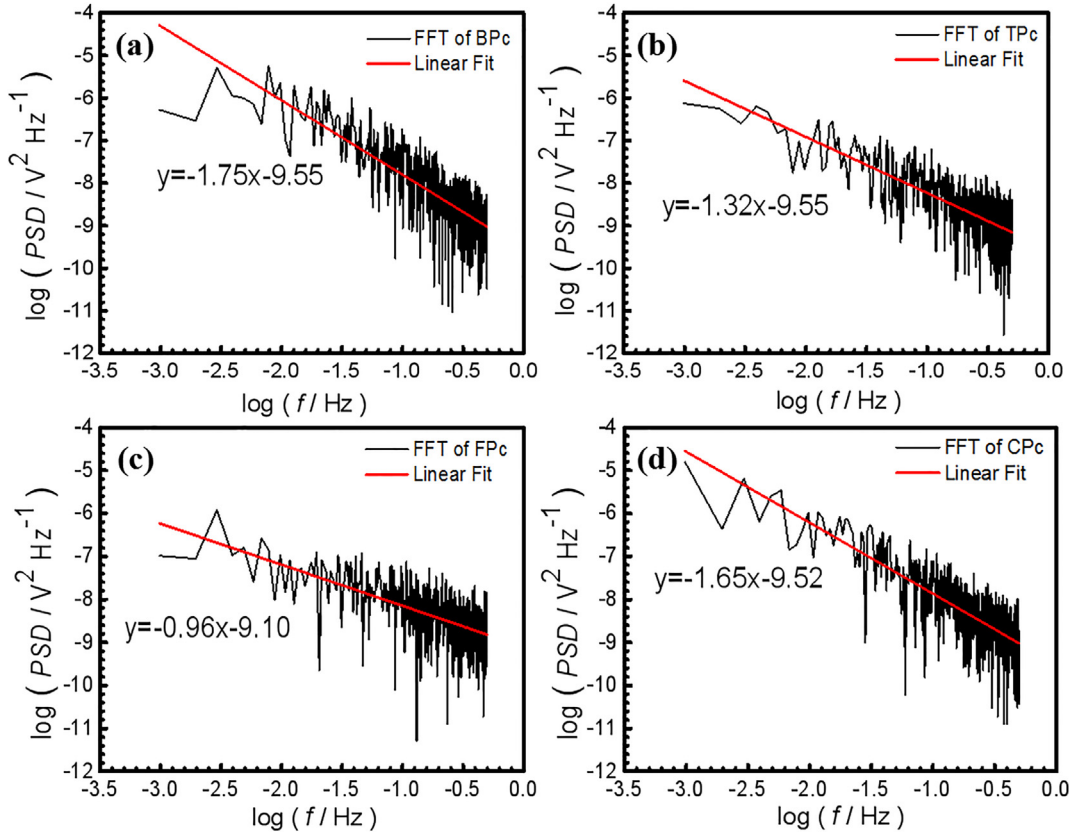

Fig. 6. PSD plots of (a) BPc, (b) TPc, (c) FPc and (d) CPc in 3.5 wt% NaCl aqueous solution after fast Fourier transform (FFT).

The potential noise after eliminating DC signal was also analyzed by fast Fourier transform (FFT) and dimensionless analysis. Power spectral density (PSD) plots of scratched aluminum sheets in 3.5 wt% NaCl aqueous solution are shown in Fig. 6. One of the most obvious features of the PSD is their slopes. In EN frequency domain analysis, it is generally thought that the relative size of the high frequency linear slope can evaluate the corrosion tendency of metals. It is believed that the large slope (small inclination) indicates the local corrosion on the electrode surface, while the small slope (large inclination) manifests that the electrode surface is in a state of uniform corrosion or passivation [32]. The calculated slopes are shown in Fig. 6, it can be observed that the slope of FPc is the largest, and the value is about −0.96. However, values of BPc and CPc are almost the same, about −1.6 ~ −1.7. The slope of TPc is sort of in between, and the value is −1.3. It is noted that substrates coated by TPc and FPc exhibit different performance from that coated by BPc and CPc, which incline to localized corrosion. In addition, the metal corrosion of specimen coated by FPc is more intense than that of TPc. The results of fast Fourier transform concur with that obtained from the potential noise analysis, confirming the

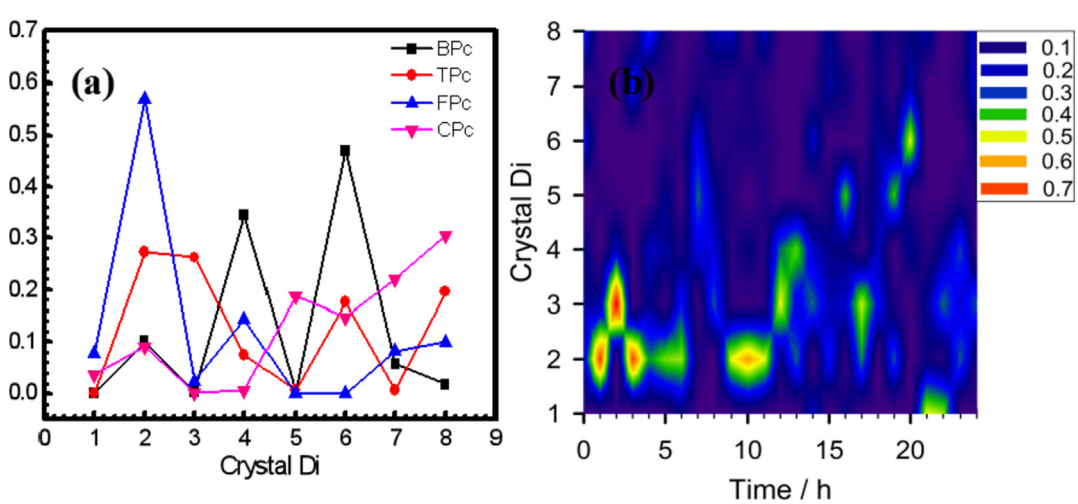

Fig. 7. (a) EDP of BPc, TPc, FPc and CPc obtained from wavelet analysis technique, (b) contour plot of the energy distribution of scratched FPc.

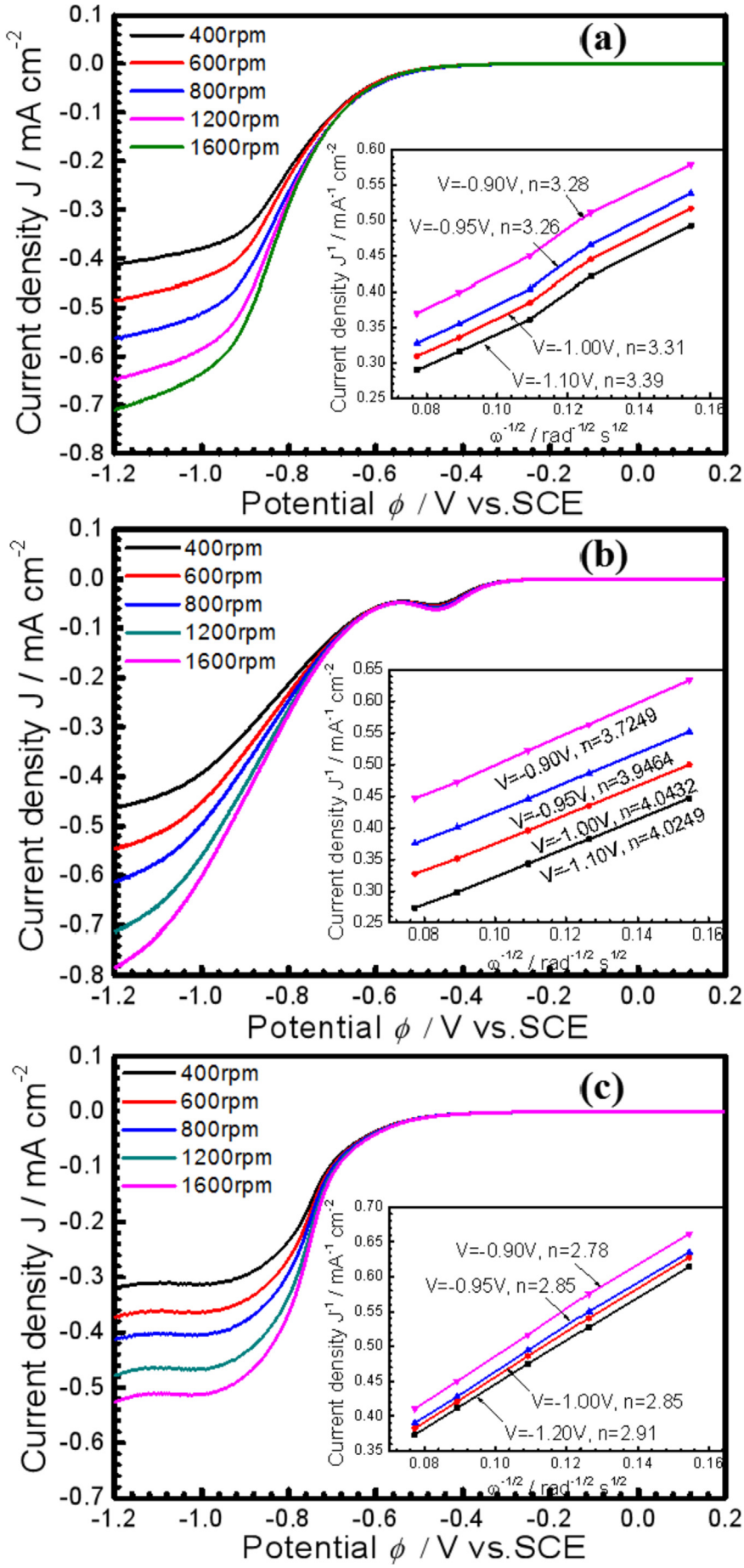

Fig. 8. LSVs for the (a) TiO_2, (b) Fe_2O_3 and (c) Cu_2O on an RDE with various rotating speeds. Inset in them are corresponding Koutecky-Levich plots at different potentials and electron transfer numbers.

corrosion-promotion activity of TPc and FPc.

Potential noise is also analyzed by the wavelet technique based on orthogonal sym4 wavelet. The characteristics of energy distribution plot (EDP) obtained from the wavelet analysis technique are "fingerprints" of the noise signal and can be used to differentiate the reaction type at the metal/electrolyte interface [33,34]. Generally, it is accepted that the initiation, growth, and death of metastable process always occur prior to corrosion, whereas corrosion is faster than other processes such as diffusion of aggressive ions or oxygen molecules [35]. The time-scale of different crystal D is ranked in an increasing order: D1 < D2 < … < D7 < D8. The relative energy distribution in crystal D1-D2, D3-D6, and D7-D8 mainly reflects the information about metastable processes, corrosion, and diffusion, respectively [36,37]. Fig. 7a shows the EDP plots of the potential noise presented in Fig. 5. The EDP of BPc and CPc show a random energy distribution mainly between D3 and D8, indicating that there are two main processes including aluminum corrosion and oxygen diffusion occurs in the aluminum/electrolyte interface at damaged coating [38]. The wavelet analysis results further reveal that the D2 value of BPc, TPc, FPc and CPc are 0.10, 0.27, 0.57 and 0.09, respectively, which also demonstrates that the substrates coated TPc, FPc are at metastable processes with a fast corrosion rate. Moreover, the corrosion-promotion activity of FPc is more furious than that of TPc. In addition, the scratched aluminum sheets coated FPc are further measured for 24 h to observe the surface reaction, and the EDP shown in Fig. 7b reveals that the energy distributes in the D2 region (fast process) during 24 h immersion. The fast process corresponds to a metastable process raised by the dissolution/formation of protective layer (aluminum passivation) [39]. The EDP results also confirm the corrosion-promotion activity of TPc and FPc.

In order to elaborate why TiO_2 and Fe_2O_3 can promote corrosion of metal substrate, a mechanism is proposed in this work. For the action of "corrosion-promotion" activity, the transition of electrons from the metal substrate to the semiconductor materials is a necessary prerequisite. According to the semiconductor physics, when a metal-semiconductor contact is formed, the characteristics of contact can be simply determined by the different work functions between metal and semiconductor [17,40]. A shallow work function metal can give an Ohmic contact to a deep work function n-type semiconductor, while a Schottky contact is formed at the interface between a deep work function metal and a shallow work function n-type semiconductor. As for p-type semiconductors, the characteristics of contact are the opposite. TiO_2 and Fe_2O_3 are n-type semiconductors, and Cu_2O is p-type semiconductor. Work functions of metal (including copper and aluminum) and semiconductor fillers were measured with Scanning Kelvin Probe, and the values of copper, aluminum, TiO_2, Fe_2O_3 and Cu_2O are 4.65 eV, 4.28 eV, 5.14 eV, 5.20 eV and 5.08 eV, respectively. It reveals an Ohmic contact is fabricated because the electron affinity of copper and aluminum is lower than that of TiO_2 or Fe_2O_3. The Ohmic contact allows electrons to transfer from copper and aluminum into TiO_2 or Fe_2O_3 at the metal/semiconductor interface. However, Cu_2O forms a Schottky contact with copper and aluminum, so that transfer of electrons cannot occur at the metal/Cu_2O interface.

Another necessary condition for implementing the "corrosion-promotion activity" is that semiconductor oxides can consume electrons quickly by a cathode reaction, which contributes to metal corrosion. RDE measurement was used to reveal the ORR kinetics of TiO_2, Fe_2O_3 and Cu_2O in 3.5 wt% NaCl solution. The linearity of the Koutecky-Levich plots and near parallelism of the fitting lines suggest first-order reaction kinetics toward the concentration of dissolved oxygen and similar electron transfer numbers for ORR at different potentials [41]. Fig. 8 reveals that the average electron transfer number of Fe_2O_3 is calculated to be ~3.9 from the multiple slopes of Koutecky-Levich plots over the potential ranging from −0.9 to −1.1 V vs SCE, suggesting a dominant four electrons reduction process. The average electron transfer number of TiO_2 and Cu_2O are ~3.3 and ~2.8 separately, suggesting TiO_2 and Cu_2O favor both two electrons and four electrons oxygen reduction processes. The catalyzed ORR would propel the copper oxidation to generate electrons. The four electrons reduction process is more conductive than the two electrons reduction process because it can promote the consumption of electrons that are conducted from the metal substrates rapidly. Such behavior will decrease the corrosion resistance of a copper substrate, which deduces that Fe_2O_3 has greater ORR catalytic activity than TiO_2 and Cu_2O, and further indicates Fe_2O_3 has more intense corrosion-promotion activity than TiO_2.

4. Conclusion

In this work, TiO_2, Fe_2O_3 and Cu_2O powders were prepared by hydrothermal methods and incorporated into PVB coatings. Then the coated metal substrates were scratched so that the semiconductor fillers can completely make contact with metal substrates at coating defects. LEIS, EIS measurements and SEM images of the scratches demonstrated that TiO_2 and Fe_2O_3 have a strong interaction with metal substrates, which possess corrosion-promotion activity that can greatly accelerate metal corrosion, while Cu_2O has little impact on corrosion behaviors of metal. The EN measurement further manifested FPc causes more intense corrosion acceleration than TPc, compared to BPc and CPc. Based on the experimental results, a micro-galvanic corrosion mechanism including work function difference and ORR activity was consequently proposed to explain the corrosion-promotion phenomenon in the study. Due to different work function, Fe_2O_3 and TiO_2 form an Ohmic contact with the metal that allows the transfer of electrons, while Cu_2O forms a Schottky contact with the metal. In addition, Fe_2O_3 has greater ORR catalytic activity than TiO_2 which propels the conduction and consumption of electrons. Moreover, the discovery could cause more careful consideration when choosing semiconductor oxides as coating fillers.

Acknowledgments

This work was supported by the National Natural Science Foundation of China (No. 51671047, 21703026, 21403030); National Key R&D Program of China (No. 2016YFB0601100); General Financial Grant from the China Postdoctoral Science Foundation (No. 2017M610177); Natural Science Foundation of Liaoning Province (No. 2015020178) and Fundamental Research Funds for the Central Universities (No. DUT16RC(3)106).

References

[1] N.M. Taher, A.S. Al Jabab, Dent. Mater. 19 (2003) 54–59.
[2] Y. Hu, K.Q. Peng, L. Liu, Z. Qiao, X. Huang, X.L. Wu, X.M. Meng, S.T. Lee, Sci. Rep. UK 4 (2014) 3667.
[3] J. Ning, Y.G. Zheng, B. Brown, D. Young, S. Nesic, Corrosion 73 (2017) 155–168.
[4] J.L. Crolet, N. Thevenot, S. Nesic, Corrosion 54 (1998) 194–203.
[5] W. Sun, S. Nesic, R.C. Woollam, Corrosion Sci. 51 (2009) 1273–1276.
[6] A. M. El-Sherik (Edt), Academic Press by Elsevier (first ed.), ISBN: 9780081011058 (2017).
[7] P.P. Bai, Y.X. Liang, S.Q. Zheng, C.F. Chen, Ind. Eng. Chem. Res. 55 (2016) 10932–10940.
[8] L.Y. Song, Z.Y. Chen, J. Electrochem. Soc. 162 (2015) C79–C84.
[9] L.Y. Song, Z.Y. Chen, B.R. Hou, Corrosion Sci. 93 (2015) 191–200.
[10] C. Chartier, S. Bastide, C. Levy-Clement, Electrochim. Acta 53 (2008) 5509–5516.
[11] H.Y. Cheung, H. Lin, F. Xiu, F.Y. Wang, S. Yip, J.C. Ho, C.Y. Wong, J. Phys. Chem. C 118 (2014) 6903–6908.
[12] S.M. Greil, J. Rappich, L. Korte, S. Bastide, ACS Appl. Mater. Interfaces 7 (2015) 11654–11659.

[13] V. Subramanian, E. Wolf, P.V. Kamat, J. Phys. Chem. B 105 (2001) 11439–11446.
[14] Y. Xu, A. Ali, K. Shehzad, N. Meng, M.S. Xu, Y.H. Zhang, X.R. Wang, C.H. Jin, H.T. Wang, Y.Z. Guo, Z.Y. Yang, B. Yu, Y. Liu, Q.Y. He, X.F. Duan, X.M. Wang, P.H. Tan, W.D. Hu, H. Lu, T. Hasan, Adv. Mater. Technol. US 2 (2017).
[15] I.G. Hill, A. Rajagopal, A. Kahn, Y. Hu, Appl. Phys. Lett. 73 (1998) 662–664.
[16] R.T. Tung, Phys. Rev. B 45 (1992) 13509–13523.
[17] J. Zhang, L. Zhang, W. Wang, L.H. Han, J.C. Jia, Z.W. Tian, Z.Q. Tian, D.P. Zhan, Chem. Sci. 8 (2017) 2407–2412.
[18] V. Ezhilselvi, J. Nithin, J.N. Balaraju, S. Subramanian, Surf. Coatings Technol. 288 (2016) 221–229.
[19] M. Kaltenbrunner, G. Adam, E.D. Glowacki, M. Drack, R. Schwodiauer, L. Leonat, D.H. Apaydin, H. Groiss, M.C. Scharber, M.S. White, N.S. Sariciftci, S. Bauer, Nat. Mater. 14 (2015) 1032.
[20] A. Kolodziejczak-Radzimska, T. Jesionowski, Materials 7 (2014) 2833–2881.
[21] W. Wu, C.Z. Jiang, V.A.L. Roy, Nanoscale 7 (2015) 38–58.
[22] R.E. Lobnig, W. Villalba, K. Goll, J. Vogelsang, I. Winkels, R. Schmidt, R. Zanger, J. Soetemann, Prog. Org. Coatings 55 (2006) 363–374.
[23] V. Stengl, J. Subrt, S. Bakardjieva, A. Kalendova, P. Kalenda, Dyes Pigments 58 (2003) 239–244.
[24] W. Sun, L.D. Wang, T.T. Wu, G.C. Liu, Corrosion Sci. 82 (2014) 1–6.
[25] W. Sun, L.D. Wang, T.T. Wu, T.Z. Zhu, H.B. Xie, Y.Q. Pan, G.C. Liu, Adv. Eng. Mater. 18 (2016) 923–931.
[26] S.L. Sinebryukhov, A.S. Gnedenkov, D.V. Mashtalyar, S.V. Gnedenkov, Surf. Coatings Technol. 205 (2010) 1697–1701.
[27] E. Cano, D. Lafuente, D.M. Bastidas, J. Solid State Electrochem. 14 (2010) 381–391.
[28] H.S. Klapper, J. Goellner, A. Heyn, Corrosion Sci. 52 (2010) 1362–1372.
[29] P.C. Pistorius, G.T. Burstein, Philos. Trans. Roy. Soc. A 341 (1992) 531–559.
[30] M. Hashimoto, S. Miyajima, T. Murata, Corrosion Sci. 33 (1992) 905–915.
[31] M.Z. Yang, M. Wilmott, J.L. Luo, Thin Solid Films 326 (1998) 180–188.
[32] U. Bertocci, F. Huet, B. Jaoul, P. Rousseau, Corrosion 56 (2000) 675–683.
[33] A. Aballe, M. Bethencourt, F.J. Botana, M. Marcos, Electrochem. Commun. 1 (1999) 266–270.
[34] R. Moshrefi, M.G. Mahjani, M. Jafarian, Electrochem. Commun. 48 (2014) 49–51.
[35] F.H. Cao, Z. Zhang, J.X. Su, Y.Y. Shi, J.Q. Zhang, Electrochim. Acta 51 (2006) 1359–1364.
[36] T. Zhang, Y.W. Shao, G.Z. Meng, F.H. Wang, Electrochim. Acta 53 (2007) 561–568.
[37] B. Zhao, J.H. Li, R.G. Hu, R.G. Du, C.J. Lin, Electrochim. Acta 52 (2007) 3976–3984.
[38] M. Shahidi, S.M.A. Hosseini, A.H. Jafari, Electrochim. Acta 56 (2011) 9986–9997.
[39] A.M. Lafront, F. Safizadeh, E. Ghali, G. Houlachi, Electrochim. Acta 55 (2010) 2505–2512.
[40] W.Y. Yang, S.W. Rhee, Appl. Phys. Lett. 91 (2007).
[41] K.J.J. Mayrhofer, D. Strmcnik, B.B. Blizanac, V. Stamenkovic, M. Arenz, N.M. Markovic, Electrochim. Acta 53 (2008) 3181–3188.